

SYMPLECTIC STRUCTURES WITH NON-ISOMORPHIC PRIMITIVE COHOMOLOGY ON OPEN 4-MANIFOLDS

MATTHEW GIBSON, LI-SHENG TSENG, AND STEFANO VIDUSSI

ABSTRACT. We analyze two different fibrations of a link complement M^3 constructed by McMullen-Taubes, and studied further by Vidussi. These examples lead to inequivalent symplectic forms ω_1 and ω_2 on $X = S^1 \times M^3$, which can be distinguished by the dimension of the primitive cohomologies of differential forms. We provide a general algorithm for computing the monodromies of the fibrations explicitly, which are needed to determine the primitive cohomologies. We also investigate a similar phenomenon coming from fibrations of a class of graph links, whose primitive cohomology provides information about the fibration structure.

1. INTRODUCTION

Given two symplectic forms ω_0 and ω_1 , there are various (differing) definitions of equivalence. In this paper, two symplectic forms are called *equivalent* if there is some combination of diffeomorphisms and smooth paths of symplectic forms interpolating between ω_0 and ω_1 . Otherwise the two forms are called *inequivalent*. Examples of inequivalent symplectic structures on closed manifolds of dimension greater than four were known for quite some time. Explicit examples were given by Ruan in [9]. The question of existence on 4-manifolds, however, was open until 1999 when McMullen and Taubes ([7]) provided the first (simply-connected) 4-manifold, proving the existence of a pair of inequivalent symplectic forms by using Seiberg-Witten and gauge theory. Their manifold is constructed from a fibered link complement. In [15], the third author found another fibration with symplectic structure inequivalent from the McMullen-Taubes pair. Shortly after, in [6], LeBrun provided even more examples of inequivalent structures on a 4-manifold using Kodaira fibrations. His construction is more explicit but comes at the cost of losing simply-connectedness. Later, Smith [10] constructed yet another family of simply-connected 4-manifolds with n -inequivalent symplectic forms, for any positive integer n .

In [13], Tseng and Yau studied a new invariant on any symplectic manifold (X^{2n}, ω) given by a cohomology $PH_{\pm}^*(X^{2n}, \omega)$ (see also [12]). Unlike the de Rham cohomology, it turns out that the dimension of this symplectic cohomology is not invariant under homeomorphism type. Let $\pi : Y_f \rightarrow S^1$ be a surface bundle with fiber an oriented finite type surface Σ with monodromy $f : \Sigma \rightarrow \Sigma$. The associated manifold $X = S^1 \times Y_f$ has a symplectic structure ω constructed in [11] as follows. Let $d\pi$ be the 1-form associated to the projection map and dt the 1-form of the S^1 factor in X . Define the symplectic form $\omega = dt \wedge d\pi + \omega_{\Sigma}$, where ω_{Σ} is a global two form on Y_f restricting to the symplectic form on each fiber. We will explain how the dimensions of $PH_{\pm}^2(X, \omega)$ count the number of Jordan blocks of size at least two in the decomposition of $f^* - 1 : H^1(\Sigma) \rightarrow H^1(\Sigma)$. This key fact allows us to distinguish different symplectic structures associated to fibrations of a 4-manifold, inspired by the construction of McMullen and Taubes in [7]. Specifically, there exist fibrations of a 3-manifold M^3 leading to inequivalent symplectic structures ω_1 and ω_2 on $X = S^1 \times M^3$. We show that the primitive cohomologies $PH_{\pm}^2(X, \omega_1)$ and $PH_{\pm}^2(X, \omega_2)$ are not isomorphic. To the authors' knowledge, this occurrence is the first example of different primitive cohomologies arising from the same 4-manifold.

We also consider another example of a fibered 3-manifold, given by a graph link. In [14], the third author constructed a class of 3-manifolds $M^{(2n)} = S^3 \setminus K^{(2n)}$, whose fibrations are given by pairs of integers (m_1, m_2) satisfying certain conditions. Here, $K^{(2n)}$ is a special type of the graph links studied generally in [3]. It was shown in [14] that the associated symplectic 4-manifold $S^1 \times M^{(2n)}$ admits at least $n + 1$ inequivalent symplectic structures. We investigate the primitive cohomology of this 4-manifold for different fibrations and show its dimension directly relates to the divisibility of the m_i 's by 3.

It is worthwhile to point out that the differential forms underlying $PH^*(X, \omega)$ have new Massey products different from the traditional Massey products on $H^*(X)$. These new Massey products can detect Jordan blocks of size exactly three (see [5] for details) and may provide a deeper understanding on the relationship between ω and f . We focus here only on the cohomology group structure as it already leads to promising results.

The structure of the paper is as follows. In Section 2, we review the basic properties of $PH^*(X, \omega)$ and the de Rham cohomology of a fibered 3-manifold. In Section 3, we discuss the details of the fibrations in [7] and use the work of [7] and [15] to show that there is an open manifold X^4 admitting two inequivalent symplectic forms ω_0, ω_1 such that $PH_+^2(X, \omega_0) \neq PH_+^2(X, \omega_1)$. The complete explanation of the setup used is given in the Appendix and Section 4, where we give explicit constructions of the monodromy of each bundle. Finally, in Section 5, we investigate a similar phenomenon for the family of fibrations on a graph link $K^{(2n)}$ introduced in [14]. In the case of $K^{(4)}$, the associated symplectic manifold $X^{(4)} = S^1 \times M^{(4)}$ has differing $\dim PH_\pm^2(X^{(4)})$ for various symplectic structures determined by the choice of the fibration of (m_1, m_2) .

Acknowledgments. The authors would like to express their thanks to Yi Liu, Curtis McMullen, Yi Ni, Nick Salter, and Jesse Wolfson for helpful conversations.

2. PRELIMINARIES

2.1. de Rham and Primitive Cohomologies.

In this section, we briefly review the basics of the de Rham cohomology of surface bundles over a circle. We then recap the primitive cohomology studied in [12] and [13], applying it to a symplectic 4-manifold associated to surface bundles.

Let $\Sigma_{g,n} = \Sigma_g - \{y_1, \dots, y_n\}$ be a Riemann surface of genus g with n points removed. When clear, the surface will simply be abbreviated by Σ . Moreover, when convenient, $P := \{y_1, \dots, y_n\}$ may be thought of as marked points. We endow Σ with a symplectic form ω_Σ and let $f : \Sigma \rightarrow \Sigma$ be any symplectic diffeomorphism preserving P setwise. Form the 3-dimensional mapping torus $Y_f = \Sigma \times [0, 1]/(x, 1) \sim (f(x), 0)$. It follows that Y_f has a Σ -bundle structure over S^1 with the projection given by $\pi : Y_f \rightarrow S^1$, $\pi([x, t]) = t$. The associated map f is called the *monodromy* of the bundle and determines the de Rham cohomology according to the Wang exact sequence

$$\cdots \longrightarrow H^0(\Sigma) \longrightarrow H^1(Y_f) \longrightarrow H^1(\Sigma) \xrightarrow{f^* - 1} H^1(\Sigma) \longrightarrow H^2(Y_f) \longrightarrow \cdots$$

This sequence yields

$$\begin{aligned} H^0(Y_f) &= \mathbb{R}, \\ H^1(Y_f) &= \ker(f^* - 1 : H^1(\Sigma) \rightarrow H^1(\Sigma)) \oplus \langle d\pi \rangle, \\ H^2(Y_f) &= \langle d\pi \rangle \wedge \operatorname{coker}(f^* - 1 : H^1(\Sigma) \rightarrow H^1(\Sigma)), \\ H^3(Y_f) &= 0, \end{aligned}$$

where $d\pi = \pi^*(d\theta)$ is the pullback under π of the volume form on S^1 .

Next we construct a symplectic manifold $X = S^1 \times Y_f$ with symplectic form $\omega = dt \wedge d\pi + \omega_\Sigma$. Here, dt is the volume form on the second S^1 factor and ω_Σ (by abuse of notation) is a global closed 2-form on Y_f which restricts to the symplectic form on each fiber. The Kunneth formula easily shows

$$\begin{aligned} H^0(X) &= \mathbb{R}, \\ H^1(X) &= \langle dt, d\pi \rangle \oplus \ker(f^* - 1 : H^1(\Sigma) \rightarrow H^1(\Sigma)), \\ H^2(X) &= \langle dt \wedge d\pi \rangle \oplus d\pi \wedge \operatorname{coker}(f^* - 1 : H^1(\Sigma) \rightarrow H^1(\Sigma)) \oplus dt \wedge \ker(f^* - 1 : H^1(\Sigma) \rightarrow H^1(\Sigma)), \\ H^3(X) &= \langle dt \wedge d\pi \rangle \wedge \operatorname{coker}(f^* - 1 : H^1(\Sigma) \rightarrow H^1(\Sigma)), \\ H^4(X) &= 0. \end{aligned}$$

Given a symplectic manifold (X^{2n}, ω) , choose a basis $\{\partial_{x^i}\}_{i=1}^{2n}$ for TX . Its differential forms $\Omega^*(X)$ carry an $sl_2(\mathbb{R})$ action, with the following sl_2 -representation:

$$\begin{aligned} L : \Omega^k(X) &\rightarrow \Omega^{k+2}(X) \\ A_k &\mapsto \omega \wedge A \end{aligned}$$

$$\begin{aligned} H : \Omega^k(X) &\rightarrow \Omega^k(X) \\ A_k &\mapsto (n - k)A_k \end{aligned}$$

$$\begin{aligned} \Lambda : \Omega^k(X) &\rightarrow \Omega^{k-2}(X) \\ A_k &\mapsto \frac{1}{2}(\omega^{-1})^{ij} \iota_{\partial_{x^i}} \iota_{\partial_{x^j}} A_k \end{aligned}$$

The *primitive forms* $\mathcal{P}^*(X)$ are the highest weight vectors in this algebra. That is, $A_k \in \mathcal{P}^k(X)$ precisely if $\Lambda A_k = 0 = \omega^{n-k+1} \wedge A_k$. This action leads to the Lefschetz decomposition so that any k -form has an expression $A_k = B_k + \omega \wedge B_{k-2} + \omega^2 \wedge B_{k-4} + \dots$ where each B_i is primitive. In [13] the authors constructed differentials $\partial_\pm : \mathcal{P}(X)^k \rightarrow \mathcal{P}^{k\pm 1}(X)$ and sequence

$$\begin{array}{ccccccccccc} 0 & \longrightarrow & \mathcal{P}^0 & \xrightarrow{\partial_+} & \mathcal{P}^1 & \xrightarrow{\partial_+} & \mathcal{P}^2 & \xrightarrow{\partial_+} & \dots & \xrightarrow{\partial_+} & \mathcal{P}^n \\ & & & & & & & & & & \downarrow \partial_+ \partial_- \\ 0 & \xleftarrow{\partial_-} & \mathcal{P}^0 & \xleftarrow{\partial_-} & \mathcal{P}^1 & \xleftarrow{\partial_-} & \mathcal{P}^2 & \xleftarrow{\partial_-} & \dots & \xleftarrow{\partial_-} & \mathcal{P}^n \end{array}$$

whose “top” and “bottom” cohomologies are denoted $PH_+^*(X, \omega)$ and $PH_-^*(X, \omega)$, respectively. Also in [12] it is proven that certain de Rham cohomological data is enough to compute the

symplectic cohomology groups $PH_{\pm}^*(X)$, given by the isomorphisms below for $k \leq n$:

(2.1)

$$PH_+^k(X) \cong \text{coker}(L : H^{k-2}(X) \rightarrow H^k(X)) \oplus \ker(L : H^{k-1}(X) \rightarrow H^{k+1}(X)),$$

(2.2)

$$PH_-^k(X) \cong \text{coker}(L : H^{2n-k-1}(X) \rightarrow H^{2n-k+1}(X)) \oplus \ker(L : H^{2n-k}(X) \rightarrow H^{2n-k+2}(X)).$$

Let us first discuss the case where ω is chosen so that $[\omega]_{dR} = [dt \wedge d\pi]_{dR}$, the more general case will be treated at the end of the section. Applying equations (2.1) and (2.2) to the 4-manifold $X = S^1 \times Y_f$, along with computations from earlier in this section, yield

$$\begin{aligned} PH_+^0(X) &\cong \mathbb{R}, \\ PH_+^1(X) &\cong H^1(X), \\ PH_+^2(X) &\cong H^2(X) / \langle dt \wedge d\pi \rangle \oplus \langle dt, d\pi \rangle \oplus [\ker(f^* - 1) \cap \text{Im}(f^* - 1)], \\ PH_-^2(X) &\cong H^2(X) \oplus [\langle dt \wedge d\pi \rangle \wedge \text{coker}(f^* - 1)] / [\langle dt \wedge d\pi \rangle \wedge \ker(f^* - 1)], \\ PH_-^1(X) &\cong H^3(X), \\ PH_-^0(X) &\cong 0. \end{aligned}$$

Let b_i denote the Betti numbers of X and $p_i^{\pm}(X, \omega)$ denote the dimensions of $PH_{\pm}^i(X, \omega)$. When the choice of the underlying symplectic structure is clear, we simply write p_i^{\pm} . Then,

$$\begin{aligned} p_0^+ &= 1, \\ p_1^+ &= b_1, \\ p_2^+ &= b_2 + 1 + \dim[\ker(f^* - 1) \cap \text{Im}(f^* - 1)], \\ p_2^- &= b_2 + \dim[\ker(f^* - 1) \cap \text{Im}(f^* - 1)], \\ p_1^- &= b_3, \\ p_0^- &= 0, \end{aligned}$$

where we have used the fact that $\dim[\ker(f^* - 1) \cap \text{Im}(f^* - 1)]$ and $\dim[(dt \wedge d\pi \wedge \text{coker}(f^* - 1)) / (dt \wedge d\pi \wedge \ker(f^* - 1))]$ are equal by realizing that both quantities count the number of Jordan blocks of $f^* - 1$ of size strictly greater than 1 (see discussion below). We note that the *primitive Euler characteristic* $\chi_p(X) = \sum (-1)^i p_i^+ - \sum (-1)^i p_i^- = 2 - b_1 + b_3$ is fixed under homeomorphism type. However, the primitive Betti numbers p_2^{\pm} may vary in general.

Let us explain how this dimension relates to the Jordan blocks of $f^* - 1$. For brevity we write $\nu_2 := \dim[\ker(f^* - 1) \cap \text{Im}(f^* - 1)]$. Now if $\alpha \in \ker(f^* - 1) \cap \text{Im}(f^* - 1)$, then $(f^* - 1)\alpha = 0$ and $(f^* - 1)\beta = \alpha$ for some β . That is, α is an eigenvector in a Jordan chain of length at least 2. It follows that ν_2 counts the number of Jordan blocks corresponding to eigenvalue $\lambda = 1$ of size *at least* 2. More generally there is a descending filtration of subgroups $PH_+^2(M) \supset J_1(M) \supset J_2(M) \supset \cdots$ where $J_k(M) = \ker(f^* - 1) \cap \text{Im}(f^* - 1)^k$. If $\alpha \in J_k(M)$, then it is the eigenvector in a Jordan chain of length at least $k+1$ given by $x_1 = \alpha$, $x_2 = (f^* - 1)^{k-1}\beta$, $x_3 = (f^* - 1)^{k-2}\beta, \dots, x_k = (f^* - 1)\beta$, $x_{k+1} = \beta$. Thus the dimension of the filtered quotient J_{k-1}/J_k counts the number of Jordan blocks of size *exactly* k .

We now consider the case where $[\omega] \neq [dt \wedge d\pi]$. Let $i : \Sigma \hookrightarrow Y_f$ be the inclusion map of the fiber and choose $\tilde{\omega}_f \in \Omega^2(Y_f)$ such that $i^*(\tilde{\omega}_f) = \omega_{\Sigma}$. Furthermore, assume $\tilde{\omega}_f$ can be chosen so that $[\omega_0] := [dt \wedge d\pi + \tilde{\omega}_f] = [dt \wedge d\pi]$. Then $PH^*(X, \omega_0)$ is given by the above computations. Given $\eta \in \Omega^1(Y_f)$ such that $d(\eta \wedge d\pi) = 0$, we can define a new symplectic form,

$\omega_\eta := \omega_0 + \eta \wedge d\pi = (dt + \eta) \wedge d\pi + \tilde{\omega}_f$. We wish to choose η so that $[\omega_\eta] \neq [\omega_0]$, which holds precisely when $[d\pi \wedge \eta] \in H^2(Y_f)$ is non-trivial. Choose a Jordan basis $\{x_{i,0}\}_{i=1}^k$ for $\ker(f^* - 1)$ and denote the corresponding Jordan chain of $x_{i,0}$ by $\{x_{i,0}, x_{i,1}, \dots, x_{i,n_i}\}$. Rearranging if necessary, we assume $n_i = 0$ for $1 \leq i \leq s$. Thus $\{x_{i,0}\}_{i=1}^s$ are the Jordan blocks of size exactly 1. Then, we can write

$$\begin{aligned} H^1(Y_f) &= \langle d\pi \rangle \oplus \langle x_{i,0} \rangle_{i=1}^k, \\ H^2(Y_f) &= \langle d\pi \wedge x_{i,n_i} \rangle_{i=1}^k, \end{aligned}$$

and express $[d\pi \wedge \eta] = \sum_{i=1}^k \lambda_i [d\pi \wedge x_{i,n_i}]$. We may write $PH_+^2(X, \omega_\eta) = H^2(X)/\langle [\omega_\eta] \rangle \oplus K_\eta$ where $K_\eta = \ker(\omega_\eta \wedge : H^1(X) \rightarrow H^3(X))$. Then

$$\begin{aligned} [\omega_\eta \wedge d\pi] &= [0], \\ [\omega_\eta \wedge dt] &= [\eta \wedge d\pi \wedge dt] = -[dt \wedge d\pi \wedge \eta], \\ [\omega_\eta \wedge x_{i,0}] &= [dt \wedge d\pi \wedge x_{i,0}]. \end{aligned}$$

We see that $[\omega_\eta \wedge (\sum_{i=1}^s \lambda_i x_{i,0} + dt)] = [dt \wedge d\pi \wedge \sum_{i=s+1}^k \lambda_i x_{i,n_i}]$, which is trivial if and only if $\eta \in \ker(f^* - 1)$. Similarly, denote by $C_\eta = \text{coker}(\omega_\eta \wedge : H^1(X) \rightarrow H^3(X))$. The above computations show $C_\eta \cong \langle dt \wedge d\pi \wedge x_{i,n_i} \rangle_{i=s+1}^k / \langle dt \wedge d\pi \wedge \eta \rangle$. The quotient by the η term will be extraneous in the case that $\eta \in \ker(f^* - 1)$. The groups $PH^*(X, \omega_\eta)$ are recorded below.

$$\begin{aligned} PH_+^0(X, \omega_\eta) &\cong H^0(X), \\ PH_+^1(X, \omega_\eta) &\cong H^1(X), \\ PH_+^2(X, \omega_\eta) &\cong H^2(X)/\langle [\omega_\eta] \rangle \oplus K_\eta, \\ PH_-^2(X, \omega_\eta) &\cong H^2(X) \oplus C_\eta, \\ PH_-^1(X, \omega_\eta) &\cong H^3(X), \\ PH_-^0(X, \omega_\eta) &\cong \langle 0 \rangle, \end{aligned}$$

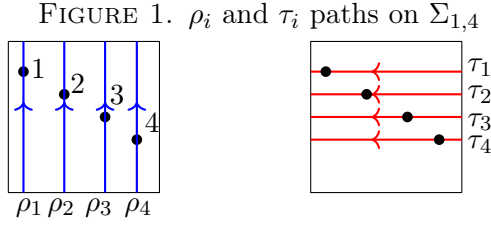
where

$$\begin{aligned} K_\eta &\cong \begin{cases} \langle d\pi \rangle \oplus \langle x_{i,0} \rangle_{i=s+1}^k, & \lambda_i \neq 0 \text{ for some } i > s \\ \langle d\pi, dt + \eta \rangle \oplus \langle x_{i,0} \rangle_{i=s+1}^k, & \lambda_i = 0 \text{ for all } i > s \end{cases} \\ C_\eta &\cong \begin{cases} \langle dt \wedge d\pi \wedge x_{i,n_i} \rangle_{i=s+1}^k / \langle dt \wedge d\pi \wedge \eta \rangle, & \lambda_i \neq 0 \text{ for some } i > s \\ \langle dt \wedge d\pi \wedge x_{i,n_i} \rangle_{i=s+1}^k, & \lambda_i = 0 \text{ for all } i > s \end{cases} \end{aligned}$$

Regardless of the class of η , we see $PH_\pm^k(X, \omega_\eta)$ are isomorphic to de Rham cohomologies for $0 \leq k \leq 1$. Furthermore, in the case that η descends to a cohomology class $[\eta] \in H^1(Y_f)$, the above computations show $\dim PH^*(X, \omega_\eta) = \dim PH^*(X, \omega_0)$. Unless otherwise stated, in the remainder of the paper we assume $[\omega] = [dt \wedge d\pi]$.

2.2. Mapping Class Group.

In this section, we review some of the necessary topics from mapping class group theory. We focus mainly on the mapping class group of $\Sigma_{1,4}$, detailing a set of generators given in [1]. We wish to study the diffeomorphisms of $\Sigma_{g,n}$ up to an equivalence. We define the *mapping class group*, denoted by $\mathcal{M}(\Sigma_{g,n})$, as the group of diffeomorphisms fixing P setwise, up to isotopies fixing P setwise. We define the *pure mapping class group*, $\mathcal{PM}(\Sigma_{g,n})$, as the subset of elements



from $\mathcal{M}(\Sigma_{g,n})$ fixing P pointwise. Since the majority of this paper takes place in $\mathcal{PM}(\Sigma_{1,4})$ we briefly discuss the diffeomorphisms generating this subgroup for the torus with four marked points. We define τ_i as the longitudinal curve which passes above y_1, y_2, \dots, y_{i-1} , through y_i , and below y_{i+1}, \dots, y_n . Denote by ρ_i the meridian curve passing through y_i .

From these curves we define homeomorphisms $\text{Push}(\tau_i)$ and $\text{Push}(\rho_i)$, called the point-pushing maps. These are classical maps in mapping class group theory. They may be loosely visualized as follows: $\text{Push}(\tau_i)$ is the map which pushes the point x_i around the curve τ_i , “dragging” the rest of the surface $\Sigma_{1,4}$ with it. $\text{Push}(\rho_i)$ has a similar interpretation. In [1], Birman showed that the push maps generate the mapping class group:

$$\mathcal{PM}(\Sigma_{1,4}) = \langle \text{Push}(\tau_i), \text{Push}(\rho_i) \rangle, i = 1, 2, 3, 4.$$

It turns out that these maps can be realized in terms of Dehn twists along homology generators for $H_1(\Sigma_{1,4})$. These explicit expressions are worked out in the Appendix. (The curves ρ_i and τ_i are pictured in Figure 1, drawn on the square representing $\Sigma_{1,4}$.)

Another important subgroup of the mapping class group is the *Torelli group*, $\mathcal{I}(\Sigma)$, consisting of diffeomorphisms acting trivially on (co)homology. Thus,

$$\mathcal{I}(\Sigma) = \{f \in \mathcal{M}(\Sigma) : 1 = f^* : H^1(\Sigma) \rightarrow H^1(\Sigma)\}.$$

Calculations in Section 2.2 show that if $f \in \mathcal{I}(\Sigma)$ then $H^*(S^1 \times Y_f) = H^*(T^2 \times \Sigma)$ and $PH^*(S^1 \times Y_f) = PH^*(T^2 \times \Sigma)$ as groups. Thus two Torelli-bundles cannot be distinguished from their primitive cohomology groups alone. However, by the same reasoning, $f \in \mathcal{I}$ and $g \notin \mathcal{I}$ can *always* be distinguished by the dimension of the cohomology groups.

3. McMULLEN-TAUBES TYPE 4-MANIFOLDS

In this section, we will discuss different presentations of a 3-manifold, the complement of a link in S^3 , as fibration with fiber a punctured torus or sphere. All the torus fiber examples will induce symplectic structures with identical primitive cohomologies but the sphere fibration will be shown to give primitive cohomology of different dimension.

We quickly review the examples constructed in [7] and [15]. In [7], McMullen and Taubes considered a 3-manifold M which is a link complement $S^3 \setminus K$. Here, K is the Borromean rings $K_1 \cup K_2 \cup K_3$ plus K_4 , the axis of symmetry of the rings. By performing 0-surgery along the Borromean rings we obtain a presentation of M as $\mathbb{T}^3 \setminus L$ where:

- $L \subset \mathbb{T}^3$ is a union of four disjoint, closed geodesics L_1, L_2, L_3, L_4 ,
- $H_1(\mathbb{T}^3) = \langle L_1, L_2, L_3 \rangle$,
- $L_4 = L_1 + L_2 + L_3$.

The fiber of M is the 2-torus with punctures coming from the L_i . The different fibration structures are captured by the Thurston ball. In [7], this ball is computed as the dual of the Newton polytope of the Alexander polynomial. Endow the ball with coordinates $\phi = (x, y, z, t)$ as in [7]. Then, the Thurston unit ball has 16 top-dimensional faces (each fibered) coming in

TABLE 1. Monodromies

Type of Face	Projection Vector v_1	Monodromy
Spherical	$(0,0,0,1)$	$\sigma_1^{-1}\sigma_2\sigma_1^{-1}\sigma_2\sigma_1^{-1}\sigma_2$
Toroidal	$(-1,-1,1)$	$\tau_3^{-1}\tau_2^{-1}\tau_1^{-1}\rho_1^{-1}\rho_2^{-1}\tau_1^{-1}\rho_2\tau_4^{-1}\rho_4^{-1}\tau_3^{-1}$
Toroidal	$(-1,1,1)$	$\rho_2^{-1}\tau_1\rho_2^{-1}\tau_1^{-1}\tau_4^{-1}\rho_3^{-2}\tau_2^{-1}\rho_4^{-1}\rho_1^{-1}$

8 pairs under the symmetry $(\phi, -\phi)$. Furthermore, restricting to faces that are dual to those vertices of the Newton polytope with no t -component, we get 14 faces, that come in two types; quadrilateral and triangular. It is shown in [7] that there exists a pair of inequivalent symplectic forms on a 4-manifold coming from different fibrations of $\mathbb{T}^3 \setminus L$. These fibrations correspond to points lying on the two distinct types of faces. In [15], it is shown that the remaining pair of $16 - 14 = 2$ faces (with a non-zero t -component) yield a third symplectic structure which is inequivalent to the two found by McMullen and Taubes.

We will investigate the monodromy of the fibration given in [15], in which it is observed that M admits a fibration with fiber the four-punctured 2-sphere. Table 1 summarizes the conclusions of the examples to follow. Determining these monodromy formulas explicitly is a crucial step in computing the dimension of $PH_{\pm}^2(X, \omega)$, since it depends on the Jordan decomposition.

The first example is the fibration with fiber $\Sigma_{0,4}$, hence ‘spherical’ type. The other two examples are of ‘toroidal’ type with fiber $\Sigma_{1,4}$. In the spherical example, the given projection vector is the cohomology class in $H^1(M^3)$ corresponding to a point on the Thurston ball. The projection vectors of the ‘toroidal’ type examples refer to the vector used in its fiber bundle construction and not the point on the Thurston ball. These details are elaborated on in the Appendix. For notational simplicity, in Table 1, $\mathcal{P}ush(\rho_i)$ and $\mathcal{P}ush(\tau_i)$ are abbreviated to ρ_i and τ_i , respectively.

Spherical Example. In this Example, we take the fibration from [15] obtained by performing 0-surgery along the K_4 axis. The fiber is S^2 punctured four-times, with monodromy given by the braid word corresponding to the Borromean rings. Let σ_i denote the half-Dehn twist which switches marked points i and $i + 1$. This homeomorphism can be viewed similar to the push map, where we “push” the surface through the arc connecting the i th and $(i + 1)$ th points. As a braid it is the element which passes the i th string over the $(i + 1)$ th string. Under this identification, the monodromy is given by

$$\sigma_1^{-1}\sigma_2\sigma_1^{-1}\sigma_2\sigma_1^{-1}\sigma_2.$$

The derivation of the toroidal type monodromies is much more involved. We carefully work out these formulas in the next section. For now, we take the monodromies from Table 1 as true and examine their cohomological implications.

3.1. Cohomological Analysis. Denote by g the monodromy from fiber the four-punctured 2-sphere $\Sigma_{0,4}$. Similarly, f denotes either of the two monodromies coming from the four-punctured torus fiber $\Sigma_{1,4}$ in Table 1. With the monodromy f , we can compute its action on $H^1(\Sigma_{1,4})$ (either by hand or with the help of software) to conclude that $\dim \ker(f^* - 1) = b_1(Y_f) - 1 = 3$ in both ‘toroidal’ cases. Let $X_f = S^1 \times Y_f$ and $X_g = S^1 \times Y_g$. By the above discussion, these manifolds are diffeomorphic, and we will compute the primitive cohomology of the symplectic structures associated to the fibrations, determined by the monodromy f and g .

With respect to the ordering $(a_0, a_1, a_2, a_3, b_0)$ of basis vectors for $H^1(\Sigma_{1,4})$, computation shows the action on $H^1(\Sigma_{1,4})$ is given by

$$f^* - 1 = \begin{pmatrix} -1 & -1 & -1 & -1 & 1 \\ 0 & 0 & 0 & 0 & -1 \\ 1 & 1 & 1 & 1 & 1 \\ 0 & 0 & 0 & 0 & -1 \\ 0 & 0 & 0 & 0 & 0 \end{pmatrix}, \quad J = \begin{pmatrix} 0 & 1 & 0 & 0 & 0 \\ 0 & 0 & 0 & 0 & 0 \\ 0 & 0 & 0 & 1 & 0 \\ 0 & 0 & 0 & 0 & 0 \\ 0 & 0 & 0 & 0 & 0 \end{pmatrix},$$

for all f . Here J is the Jordan matrix for $f^* - 1$. We note it has two blocks of size 2 and one of size 1. It follows that

$$\begin{aligned} \ker(f^* - 1) &= \langle (1, 0, 0, -1, 0), (0, 1, 0, -1, 0), (0, 0, 1, -1, 0) \rangle, \\ \text{Im}(f^* - 1) &= \langle (-1, 0, 1, 0, 0), (1, -1, 1, -1, 0) \rangle. \end{aligned}$$

A quick check shows

$$(f^* - 1)(-1, 0, 1, 0, 0) = 0 = (f^* - 1)(1, -1, 1, -1, 0).$$

Hence, we conclude

$$\dim \ker(f^* - 1) \cap \text{Im}(f^* - 1) = \dim \text{Im}(f^* - 1) = 2.$$

Notice this dimension agrees with the number of blocks from J of size at least 2. Computations from Section 2 show

$$p_2^+(X_f, \omega_\eta) = \begin{cases} 9, & \lambda_i \neq 0 \text{ for some } i > s \\ 10, & \lambda_i = 0 \text{ for all } i > s \end{cases}$$

We now turn to X_g . Since X_f is diffeomorphic to X_g , we must have

$$b_1(X_f) = b_1(X_g) \implies \dim \ker(g^* - 1) = \dim \ker(f^* - 1) = 3.$$

Moreover, using the formula $\chi(\Sigma_{g,n}) = 2 - 2g - n$, it follows $\chi(\Sigma_{0,4}) = -2 = 1 - b_1(\Sigma_{0,4})$, and so $b_1(\Sigma_{0,4}) = 3$. But by Rank-Nullity, $3 = 3 + \dim \text{Im}(g^* - 1)$, from which it follows $\dim \ker(g^* - 1) \cap \text{Im}(g^* - 1) = 0$. Thus $p_2^+(X_g, \omega_\eta) = b_2(X_g) + 1 = 8 \neq p_2^+(X_f, \omega_\eta)$.

We point out that from the Jordan form of the f , these monodromies are not Torelli elements of $\mathcal{M}(\Sigma_{1,4})$. However, by dimension considerations, we saw $\dim \text{Im}(g^* - 1) = 0$ and so g is a Torelli element of $\mathcal{M}(\Sigma_{0,4})$. Moreover, even though each f, f' coming from fiber $\Sigma_{1,4}$ are not Torelli, $f^* = f'^*$ and so it follows that $f'f^{-1}$ is a Torelli element.

These calculations give the following theorem.

Theorem 3.1. *There exist fibrations Y_f and Y_g of the 3-manifold M with inequivalent associated symplectic 4-manifolds $(X_f, \omega_1), (X_g, \omega_2)$, which can be distinguished by primitive cohomologies. In particular,*

$$p_2^+(X_f, \omega_1) \neq p_2^+(X_g, \omega_2).$$

To establish Theorem 3.1, it only remains to verify the toroidal type monodromies in Table 1.

4. CONSTRUCTION OF MONODROMIES

In this section, we provide details for the construction of the toroidal monodromies in Table 1. The Appendix gives an even more specific outline of the procedure that follows. In the examples to come, we take different bases $v_1 = (a_1, a_2, a_3)$, $v_2 = (1, 1, 0)$, $v_3 = (0, 1, 1)$ and fiber along v_1 so that the fiber at time t looks like $\Sigma_{t,4} = tv_1 + \langle v_2, v_3 \rangle$ with marked points

$$\begin{aligned} y_1(t) &= (-4\epsilon, 3\epsilon) + (a_3 - a_2, -a_3)t, \\ y_2(t) &= (-\epsilon, 2\epsilon) + (-a_1, a_1 - a_2)t, \\ y_3(t) &= (0, 0) + (a_3 - a_2, a_1 - a_2)t, \\ y_4(t) &= (\epsilon, -3\epsilon) + (-a_1, -a_3)t. \end{aligned}$$

Here, ϵ is some small fixed constant used to shift the marked points away from the origin at $t = 0$. The vector v_1 is the projection vector given in column 2 of Table 1. The general idea is as follows,

- (1) Using the paths of the punctures y_i , find relative locations to determine if y_i passes above or below y_j .
- (2) Express $\mathcal{P}ush(y_i(t))$ of the y_i path in terms of generators $\mathcal{P}ush(\rho_i)$, $\mathcal{P}ush(\tau_i)$.
- (3) Calculate the intersection points of punctures $(y_i(t), y_j(t))$ at times (t_i, t_j) . If $t_i > t_j$ then y_i crosses over y_j . If $t_i < t_j$ then y_j crosses over y_i .
- (4) Use the crossings information to determine the order of $\mathcal{P}ush(y_i(t))$ maps in the final monodromy.

The procedure is best demonstrated through examples. As before, we drop the push notation so that $\mathcal{P}ush(\rho_2)\mathcal{P}ush(\tau_1)^{-1}\mathcal{P}ush(\tau_3)$ is simply denoted by $\rho_2\tau_1^{-1}\tau_3$. We also use function notation right to left so that the previous word indicates y_3 travels along τ_3 then y_1 along the inverse of τ_1 then finally y_2 along ρ_2 . Homeomorphism type of the below examples was confirmed with SnapPea ([2]).

Toroidal Example 1. $v_1 = (-1, -1, 1)$

The paths of the corresponding marked points are

$$\begin{aligned} y_1(t) &= (-4\epsilon, 3\epsilon) + (2, -1)t, \\ y_2(t) &= (-\epsilon, 2\epsilon) + (1, 0)t, \\ y_3(t) &= (0, 0) + (2, 0)t, \\ y_4(t) &= (\epsilon, -3\epsilon) + (1, -1)t. \end{aligned}$$

Thus y_2 and y_3 travel in a parallel horizontal direction. y_1 and y_4 travel downwards and to the right and so will intersect both y_2 and y_3 . We first find these intersection times. We illustrate the process for y_1 and y_3 and summarize the other points in Table 2. We need times t_1 and t_3 so that $y_1(t_1) = y_3(t_3)$. In other words, we seek a solution to the system

$$\begin{aligned} -4\epsilon + 2t_1 &= 2t_3, \\ 3\epsilon - t_1 &= 0, \end{aligned}$$

which gives $(t_1, t_3) = (3\epsilon, \epsilon + \frac{n}{2})$, $n = 0, 1$. Hence y_1 and y_3 intersect twice. The first time y_1 passes over y_3 . Then at $t_3 = \epsilon + \frac{1}{2}$, y_3 crosses y_1 . At $t_2 = \frac{5}{8}\epsilon + \frac{1}{2}$, y_2 passes over y_1 . Similarly solving the corresponding system for y_2 and y_3 yields $(t_2, t_3) = (\frac{2}{3}\epsilon + \frac{n}{2}, 1 - \frac{1}{3}\epsilon)$, $n = 0, 1$. Both y_2 times occur before y_3 , hence we conclude y_3 passes over y_2 twice. The remaining points of

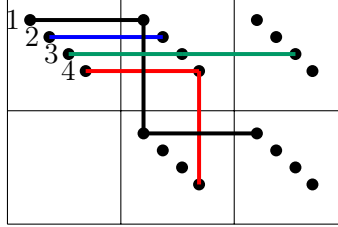
intersection are given in Table 2. The times specified are the later of the two crossing times and the points have been listed in order of intersection occurrence, from first to last.

TABLE 2. Toroidal Example 1 Intersections

Points	Time	Crossing
(y_1, y_3)	3ϵ	y_1 over y_3
(y_1, y_3)	$\epsilon + \frac{1}{2}$	y_3 over y_1
(y_2, y_4)	$1 - 3\epsilon$	y_2 over y_4
(y_3, y_4)	$1 - 3\epsilon$	y_4 over y_3
(y_1, y_2)	$1 - \epsilon$	y_2 over y_1
(y_1, y_4)	$1 - \epsilon$	y_1 over y_4
(y_3, y_4)	$1 - \epsilon$	y_3 over y_4

Pictured in Figure 2 are the paths of the y_i drawn in the plane (up to identification), where we have decomposed the “diagonal” paths of y_1 and y_4 into a combination of basis curves ρ_i and τ_i . To find the path of y_1 , for example, we must use its velocity vector $(2, -1)$ as well as the relative locations of y_1 with respect to the start points of y_2 , y_3 , and y_4 . Given that point y_2 starts at $(-\epsilon, 2\epsilon)$, we have $y_1(\frac{3}{2}\epsilon) = (-\epsilon, \frac{3}{2}\epsilon)$ and so y_1 travels ‘below’ the y_2 start point. Similar computations show y_1 travels above both the y_3 and y_4 start points. As illustrated in Figure 2, the velocity vector $(2, -1)$ suggests y_1 has a path given by $\tau_1^{-1}\rho_1^{-1}\tau_1^{-1}$. However the diagonal path homotopic to this combination will not preserve the condition that y_1 travels below the y_2 start point. To remedy this situation, we must begin the y_1 monodromy with the loop C_{12} . This curve travels counterclockwise from y_1 , enclosing y_2 . Figure 3 illustrates the $\tau_1^{-1}C_{12}$ portion of the monodromy.

FIGURE 2. Example 1 Marked Point Paths



y_4 is the only other diagonal path. We can easily check that it travels above the y_1 , y_2 , and y_3 start points. Hence its path is simply given by $\tau_4^{-1}\rho_4^{-1}$, indicated by the $(1, -1)$ velocity vector.

FIGURE 3. C_{12} Path in Example 1

Summarizing, the monodromies of the punctures are given by

$$\begin{aligned} y_1(t) : \tau_1^{-1} \rho_1^{-1} \tau_1^{-1} C_{12} &= \tau_1^{-1} \rho_1^{-1} \rho_2^{-1} \tau_1^{-1} \rho_2, \\ y_2(t) : \tau_2^{-1}, \\ y_3(t) : \tau_3^{-2}, \\ y_4(t) : \tau_4^{-1} \rho_4^{-1}. \end{aligned}$$

Now, we must determine the order of these individual monodromies in the final map. Using the above formulas, it's clear $y_2(t)$ and $y_3(t)$ are parallel so their relative order to each other in the final monodromy doesn't matter. From Table 1, we see every other point crosses over y_3 first, but then y_3 crosses over y_1 and y_4 again later. Thus we should put one τ_3^{-1} at the beginning of the monodromy and the other τ_3^{-1} at the end. Next, both y_1 and y_2 cross over y_4 so the y_4 term should come next.

It only remains to determine the order of y_1 and y_2 , which is given by Table 1 as y_1 then y_2 . Therefore our monodromy has the formula $y_3 \circ y_2 \circ y_1 \circ y_4 \circ y_3$, where the first and last y_3 terms are each a τ_3^{-1} . This ordering gives 10 possible crossings, but y_2 and y_3 are parallel and y_3 appears twice. Hence the number reduces to $10 - 3 = 7$, matching the occurrences in Table 2.

Piecing all the arguments together shows the final monodromy is isotopic to

$$\tau_3^{-1} \tau_2^{-1} (\tau_1^{-1} \rho_1^{-1} \tau_1^{-1} C_{12}) \tau_4^{-1} \rho_4^{-1} \tau_3^{-1} = \tau_3^{-1} \tau_2^{-1} (\tau_1^{-1} \rho_1^{-1} \rho_2^{-1} \tau_1^{-1} \rho_2) \tau_4^{-1} \rho_4^{-1} \tau_3^{-1}.$$

Toroidal Example 2. $v_1 = (-1, 1, 1)$

The paths of the punctures are given by

$$\begin{aligned} y_1(t) &= (-4\epsilon, 3\epsilon) + (0, -1)t, \\ y_2(t) &= (-\epsilon, 2\epsilon) + (1, -2)t, \\ y_3(t) &= (0, 0) + (0, -2)t, \\ y_4(t) &= (\epsilon, -3\epsilon) + (1, -1)t. \end{aligned}$$

Implementing the techniques from the previous example, we obtain the intersections in Table 3. There is only one non-trivial diagonal path, given by y_2 . Evaluating this path at the appropriate times yields

$$\begin{aligned} y_2(-3\epsilon) &= (-4\epsilon, 8\epsilon), \\ y_2(\epsilon) &= (0, 0), \\ y_2(2\epsilon) &= (\epsilon, -2\epsilon). \end{aligned}$$

We see that y_2 travels above y_1 and y_4 start points and through y_3 at the origin. We note at $t = \epsilon$, $y_3(\epsilon) = (0, -2\epsilon)$ has traveled away from the origin and so $y_2(t)$ and $y_3(t)$ do not actually collide. Thus, in between $\rho_2^{-1} \rho_2^{-1} \tau_2^{-1}$, we must insert a loop traveling counterclockwise starting at y_2 and enclosing y_1 . It turns out this curve is also homotopic to C_{12} (see [1] for more discussion). By drawing a diagram similar to Figure 2 one can see the correct placement

should be $\rho_2^{-1}C_{12}\rho_2^{-1}\tau_2^{-1}$. The paths of the other points are straightforward, given by

$$\begin{aligned} y_1 &: \rho_1^{-1}, \\ y_2 &: \rho_2^{-1}C_{12}\rho_2^{-1}\tau_2^{-1} = \rho_2^{-1}\tau_1\rho_2^{-1}\tau_1^{-1}\tau_2^{-1}, \\ y_3 &: \rho_3^{-2}, \\ y_4 &: \tau_4^{-1}\rho_4^{-1}. \end{aligned}$$

The ordering for this example is similar to that of Example 1; this time we need to split both of the paths y_2 and y_4 into two parts each. Notice from the individual monodromies that y_1 and y_3 are parallel so their relative order doesn't matter. We proceed by considering the remaining interactions separately. Since y_1 passes under for all its crossings, it appears first. Then y_3 over y_2 and y_2 over y_4 suggests the ordering $y_3 \circ y_2 \circ y_4$. However, we need y_4 to cross over y_3 and this current arrangement does the opposite. Hence we must split the y_4 monodromy into two components: $y_4 \circ y_3 \circ y_2 \circ y_4$. Finally, if we leave y_2 together, we will have both y_4 and y_2 crossing over one another at different times. Consequently, we also split y_2 for the ultimate ordering given by $y_2 \circ y_4 \circ y_3 \circ y_2 \circ y_4 \circ y_1$. The final monodromy pieces together as

$$y_2 \circ \tau_4^{-1} \circ \rho_3^{-2} \circ y_2 \circ \rho_4^{-1} \circ \rho_1^{-1}.$$

To reiterate, we are required to separate y_2 such that the τ_4^{-1} does not intersect the first term. This obstruction suggests the first y_2 part is τ_2^{-1} and the second term is the remaining $\rho_2^{-1}C_{12}\rho_2^{-1}$. This construction yields the desired map

$$\rho_2^{-1}C_{12}\rho_2^{-1}\tau_4^{-1}\rho_3^{-2}\tau_2^{-1}\rho_4^{-1}\rho_1^{-1}.$$

TABLE 3. Toroidal Example 2 Intersections

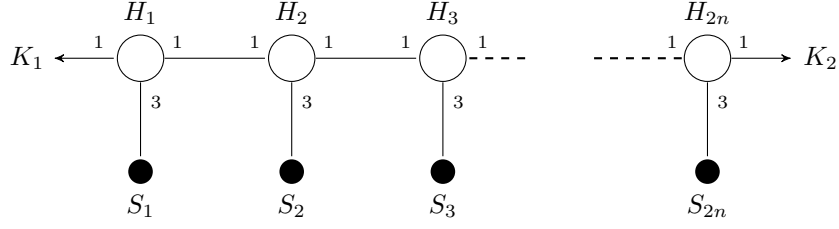
Points	Time	Crossing
(y_2, y_4)	3ϵ	y_2 over y_4
(y_2, y_3)	$\frac{1}{2}$	y_3 over y_2
(y_1, y_4)	$1 - 5\epsilon$	y_4 over y_1
(y_1, y_2)	$1 - 3\epsilon$	y_2 over y_1
(y_3, y_4)	$1 - \epsilon$	y_4 over y_3

5. ANOTHER EXAMPLE USING GRAPH LINKS

Here, we give another example of fibrations of a 3-manifold giving inequivalent symplectic structures on its associated (symplectic) 4-manifold $S^1 \times Y_f$. Let $M^{(2n)} = S^3 \setminus K^{(2n)}$, where $K^{(2n)}$ is the graph link pictured in Figure 4 below. The details of this diagram are given in [14], where the third author showed the existence of $n + 1$ inequivalent symplectic structures coming from different fibrations of $M^{(2n)}$. A fibration of $M^{(2n)}$ is given by a choice of $(m_1, m_2) \in H^1(S^3 \setminus K^{(2n)}), \mathbb{Z} \cong \mathbb{Z}^2$ satisfying the equations

$$3^i m_1 + 3^{2n-i+1} m_2 \neq 0, \text{ for all } 1 \leq i \leq 2n.$$

Details for such a fibration (and graph link theory in general) are worked out in [3]. In particular, let h denote the monodromy and h_* the induced map on homology of the fiber. [3, Theorem 13.6] shows there is an integer q such that $(h_*^q - 1)^2 = 0$. Thus the Jordan decomposition of h_* only has blocks of size 1 or 2. Furthermore, with the same q , [3] computes the characteristic polynomial of $h_*|_{Im(h_*^q - 1)}$, denoted $\Delta'(t)$. It turns out that the roots of $\Delta'(t)$ correspond to the

FIGURE 4. Diagram of $K^{(2n)}$

eigenvalues of h_* with size 2 Jordan blocks. Moreover the multiplicity of each root λ_i in $\Delta'(t)$ gives the number of size 2 blocks for λ_i .

We first introduce some notation which will be used in the definition of $\Delta'(t)$. Fix a fibration (m_1, m_2) . Let $\mathcal{E} = \{E_1, \dots, E_{2n-1}\}$ be the set of edges connecting the white nodes in Figure 4. Specifically, edge E_i connects nodes labeled H_i and H_{i+1} . For each $E_i \in \mathcal{E}$, we define an integer d_{E_i} as follows. Take the path in $K^{(2n)}$ from the arrowhead of K_1 to halfway through edge E_i (passing through nodes H_1, H_2, \dots, H_i). Let $\ell_{E_i,1}$ denote the product of all weights on edges not contained in the path but are adjacent to vertices in the path. Similarly we can take the path from the arrowhead of K_2 to halfway through edge E_i and define $\ell_{E_i,2}$ analogously. Set

$$d_{E_i} = \gcd(m_1 \ell_{E_i,1}, m_2 \ell_{E_i,2}).$$

Using Figure 4 as reference, we can easily compute that $\ell_{E_i,1} = 3^i$ and $\ell_{E_i,2} = 3^{2n-i}$. This simplifies the formula for d_E to

$$(5.1) \quad d_{E_i} = \gcd(3^i m_1, 3^{2n-i} m_2).$$

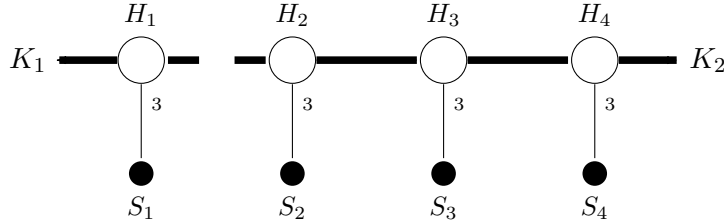
For each vertex H_i , we define an integer d_{V_i} by the formula

$$(5.2) \quad d_{V_i} = \begin{cases} \gcd(d_{E_{i-1}}, d_{E_i}), & 1 < i < 2n \\ \gcd(m_1, d_{E_1}), & i = 1 \\ \gcd(m_2, d_{E_{2n-1}}), & i = 2n \end{cases}$$

With these definitions in place, the (restricted) characteristic polynomial takes the form

$$\Delta'(t) = (t^d - 1) \prod_{i=1}^{2n-1} (t^{d_{E_i}} - 1) / \prod_{i=1}^{2n} (t^{d_{V_i}} - 1),$$

where $d = \gcd(m_1, m_2)$. To obtain a more concrete equation, we analyze several fibrations of $K^{(4)}$. Figure 5 demonstrates how $d_{E_1} = \gcd(3m_1, 3^3 m_2)$ is calculated. In particular, define

FIGURE 5. Paths $\ell_{E_1,1}$ and $\ell_{E_1,2}$ of d_{E_1}

$X^{(4)} = S^1 \times M^{(4)}$ and let $\deg \Delta'(t)$ denote the degree of the restricted characteristic polynomial

$\Delta'(t)$. Since $\deg \Delta'(t)$ is the number of Jordan blocks of size 2, which equals the number of blocks of size *at least* 2, it follows

$$\begin{aligned} p_2^+ &= b_2(X^{(4)}) + 1 + \deg \Delta'(t), \\ p_2^- &= b_2(X^{(4)}) + \deg \Delta'(t). \end{aligned}$$

In the case of a fibration represented by coprime (m_1, m_2) , there are two possibilities: 3 divides exactly one of m_1 or m_2 , or 3 neither divides m_1 nor m_2 . It turns out p_2^+ can distinguish these two possibilities and in the first case provides information about the power of 3 dividing m_1 or m_2 . We give the exact statement below.

Theorem 5.1. *Let (m_1, m_2) be coprime, representing a fibration of $M^{(4)}$. By reversing the roles of m_1 and m_2 if necessary, we write $m_1 = 3^k q$ with $\gcd(q, 3) = 1$ and assume $\gcd(3, m_2) = 1$. It follows that*

$$p_2^+ = \begin{cases} b_2(X^{(4)}) + 9, & k = 0 \\ b_2(X^{(4)}) + 7, & k = 1 \\ b_2(X^{(4)}) + 19, & k = 2 \\ b_2(X^{(4)}) + 1, & k \geq 3 \end{cases}$$

Proof. We proceed by cases, treating $k = 0$ and $k > 0$ separately.

Case 1. ($k > 0$)

Using formulas (5.1) and (5.2) we compute

$$\begin{aligned} d_{E_1} &= \gcd(3^{k+1}q, 3^3s) = \min(3^{k+1}, 3^3), \\ d_{E_2} &= \gcd(3^{k+2}q, 3^2s) = 3^2, \\ d_{E_3} &= \gcd(3^{3+k}q, 3s) = 3, \\ d_{V_1} &= \gcd(3^kq, \min(3^{k+1}, 3^3)) = \min(3^k, 3^3), \\ d_{V_2} &= \gcd(\min(3^{k+1}, 3^3), 3^2) = \min(3^{k+1}, 3^2) = 3^2, \\ d_{V_3} &= \gcd(3^2, 3) = 3, \\ d_{V_4} &= \gcd(s, 3) = 1. \end{aligned}$$

from which it follows

$$\begin{aligned} \Delta'(t) &= \frac{(t-1)(t^3-1)(t^9-1)(t^{\min(3^{k+1}, 3^3)}-1)}{(t-1)(t^3-1)(t^{\min(3^k, 3^3)}-1)(t^9-1)} \\ &= \frac{t^{3^2 \min(3^{k-1}, 3)} - 1}{t^{3 \min(3^{k-1}, 3^2)} - 1} \\ &= \begin{cases} t^6 + t^3 + 1, & k = 1 \\ t^{18} + t^9 + 1, & k = 2 \\ 1, & k \geq 3 \end{cases} \end{aligned}$$

Case 2. $\gcd(m_1, m_2) = \gcd(m_1, 3) = \gcd(m_2, 3) = 1$. Applying a similar analysis as in Case 1 shows

$$\begin{aligned} d_{E_1} &= \gcd(3, 3^3) = 3, \\ d_{E_2} &= \gcd(3^2, 3^2) = 3^2, \\ d_{E_3} &= \gcd(3^3, 3) = 3, \\ d_{V_1} &= \gcd(m_1, 3) = 1, \\ d_{V_2} &= \gcd(3, 3^2) = 3, \\ d_{V_3} &= \gcd(3^2, 3) = 3, \\ d_{V_4} &= \gcd(3, m_2) = 1, \end{aligned}$$

$$\begin{aligned} \Delta'(t) &= \frac{(t-1)(t^3-1)^2(t^9-1)}{(t-1)^2(t^3-1)^2} \\ &= \frac{t^9-1}{t-1} = (t^2+t+1)(t^6+t^3+1) \end{aligned}$$

Using the formula for p_2^+ and $\deg \Delta'(t)$ for each k from the above cases produces the claimed dimensions. \square

We conclude with some remarks. Theorem 5.1 uses $K^{(4)}$ as a matter of explicitness for factoring $\Delta(t)$ and $\Delta'(t)$. One could also consider other $K^{(2n)}$ to reach similar conclusions. For $K^{(4)}$, it can be shown that every possible value of p_2^+ , in Theorem 5.1, may be achieved for fibrations coming from any of the faces on the Thurston ball.

APPENDIX

Here we provide the details of setting up the fibration structure and converting monodromies appropriately so that they can be entered into SnapPea. Let \mathbb{T}^3 denote the 3-torus. We view it as the cube $[0, 1]^3$ under the identification $(x, y, z) \sim (x+p, y+q, z+r)$ for integers p, q, r . The axes i, j, k and their sum $i+j+k$ form four lines in the cube L_1, L_2, L_3, L_4 , respectively. By choosing different bases (v_1, v_2, v_3) for the cube and displacing the four lines we may fiber $\mathbb{T}^3 - \{L_1, L_2, L_3, L_4\}$ in different ways as follows. First we shift the four lines from the origin by

$$\begin{aligned} L_1 &= (x, -\epsilon, 3\epsilon), \\ L_2 &= (\epsilon, y, -3\epsilon), \\ L_3 &= (-\epsilon, \epsilon, z), \\ L_4 &= (x = y = z). \end{aligned}$$

Next we choose a basis $v_1 = (a_1, a_2, a_3)$, $v_2 = (1, 1, 0)$, $v_3 = (0, 1, 1)$. Initially v_1 may be any vector which gives a non-zero determinant, specifically, $a_1 - a_2 + a_3 \neq 0$. For brevity, let us denote $A := \det(v_1, v_2, v_3) = a_1 - a_2 + a_3$. Choosing to fiber along v_1 , each fiber has the form $\Sigma_t = tv_1 + \alpha v_2 + \beta v_3$ for $t \in [0, 1]$. Σ_t is \mathbb{T}^2 with four punctures denoted $x_1(t), x_2(t), x_3(t), x_4(t)$ coming from the respective lines L_i . To verify that each line L_i intersects the fiber exactly once

we must solve the following system of equations:

$$\begin{aligned} L_1 : \begin{pmatrix} 1 & 1 \\ 0 & 1 \end{pmatrix} \begin{pmatrix} \alpha \\ \beta \end{pmatrix} &= \begin{pmatrix} -\epsilon - ta_2 \\ 3\epsilon - ta_3 \end{pmatrix} \\ L_2 : \begin{pmatrix} 1 & 0 \\ 0 & 1 \end{pmatrix} \begin{pmatrix} \alpha \\ \beta \end{pmatrix} &= \begin{pmatrix} \epsilon - ta_1 \\ -3\epsilon - ta_3 \end{pmatrix} \\ L_3 : \begin{pmatrix} 1 & 0 \\ 1 & 1 \end{pmatrix} \begin{pmatrix} \alpha \\ \beta \end{pmatrix} &= \begin{pmatrix} -\epsilon - ta_1 \\ \epsilon - ta_2 \end{pmatrix} \\ L_4 : \begin{pmatrix} 0 & -1 \\ 1 & -1 \end{pmatrix} \begin{pmatrix} \alpha \\ \beta \end{pmatrix} &= \begin{pmatrix} t(a_2 - a_1) \\ t(a_3 - a_1) \end{pmatrix} \end{aligned}$$

Solving these systems for the (α, β) coordinates of the marked points $x_i(t)$ yields

$$\begin{aligned} x_1(t) &= (-4\epsilon, 3\epsilon) + (a_3 - a_2, -a_3)t, \\ x_2(t) &= (\epsilon, -3\epsilon) + (-a_1, -a_3)t, \\ x_3(t) &= (-\epsilon, 2\epsilon) + (-a_1, a_1 - a_2)t, \\ x_4(t) &= (0, 0) + (a_3 - a_2, a_1 - a_2)t. \end{aligned}$$

To align with the notation of [1], we relabel the points with respect to their first coordinate position, in increasing order, as $y_1(t) = x_1(t)$, $y_2(t) = x_3(t)$, $y_3(t) = x_4(t)$, $y_4(t) = x_2(t)$. Under this new setting the formulas for the points become

$$\begin{aligned} y_1(t) &= (-4\epsilon, 3\epsilon) + (a_3 - a_2, -a_3)t, \\ y_2(t) &= (-\epsilon, 2\epsilon) + (-a_1, a_1 - a_2)t, \\ y_3(t) &= (0, 0) + (a_3 - a_2, a_1 - a_2)t, \\ y_4(t) &= (\epsilon, -3\epsilon) + (-a_1, -a_3)t. \end{aligned}$$

Next we verify that none of the $y_i(t)$ intersect for any value of t . Notice y_2 and y_3 have the same second component in the t variable but differ by the ϵ -term constant so they will never intersect. We can apply a similar argument to the pairs (y_1, y_3) , (y_1, y_4) , and (y_2, y_4) . Lastly, by considering the (separate) systems of equations $y_1(t) = y_2(t)$ and $y_3(t) = y_4(t)$, one can easily see no solutions exist.

Let $\Sigma_{1,4}$ be the 2-torus with four punctures and $\text{Mod}(\Sigma_{1,4})$ its mapping class group (which fixes the punctures setwise). Furthermore let $\mathcal{P}\text{Mod}(\Sigma_{1,4})$ denote the *pure* mapping class group, the set of mapping class elements fixing the punctures pointwise. We set

$$(5.3) \quad H_1(\Sigma) = \langle a_0, a_1, a_2, a_3, b_0 \rangle,$$

where a_i is the homology curve between punctures i and $i + 1$ for $i > 0$ and a_0 is between marked point 1 and 4. b_0 is the homology longitudinal curve, not enclosing any punctures. These curves have algebraic intersection numbers $a_i \cdot a_j = 0$ for $i \neq j$ and $a_i \cdot b_0 = 1$. [1] introduces the following elements (pictured below) and show Dehn twists along them generate the pure mapping class group. In our setting we have $\mathcal{P}\text{Mod}(\Sigma_{1,4}) = \langle \mathcal{P}ush(\rho_i), \mathcal{P}ush(\tau_i) \rangle$, $1 \leq i \leq 4$. Here, $\mathcal{P}ush(\gamma)$ is the point pushing map along γ . We also summarize some of the important relations to be used later:

$$\begin{aligned} [\tau_i, \tau_j] &= [\rho_i, \rho_j] = 1, \\ A_{ij} &= \rho_i \tau_j^{-1} \rho_i^{-1} \tau_j, \quad C_{ij} = \tau_i \rho_j^{-1} \tau_i^{-1} \rho_j, \\ &\text{for } 1 \leq i < j < k \leq 4. \end{aligned}$$

For a more in depth discussion and outline of a proof for these identities, see [1]. We note that

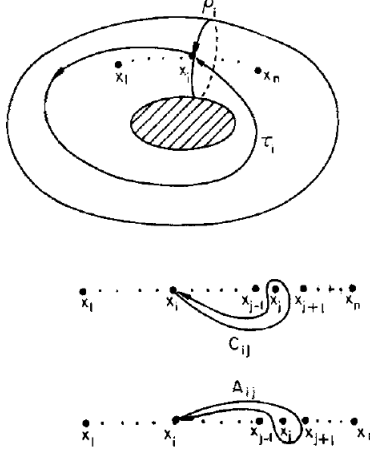


FIGURE 6. Diagram of generators taken from [1]

the formulas here differ slightly from [1] as our choice of orientation is not the same. Moreover, we use functional composition, (right to left) as opposed to algebraic. In order to use SnapPea ([2]), we need to express $\mathcal{P}ush(\rho_i)$ and $\mathcal{P}ush(\tau_i)$ in terms of Dehn twists along the curves in (5.3). The trick is to use the following fact (4.7 proven in [4]), which states

Fact. Let α be a simple loop in a surface S representing an element of $\pi_1(S, x)$, Then $\mathcal{P}ush([\alpha]) = T_a T_b^{-1}$, where a and b are isotopy classes of the simple closed curves in $S - x$ obtained by pushing α off itself to the left and right, respectively.

That is, we take an annular neighborhood of α bounded by curves a and b and then take the product of their Dehn and inverse Dehn twists, respectively. From this construction, we can immediately obtain that

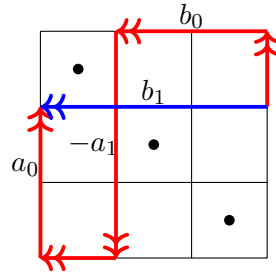
$$(5.4) \quad \mathcal{P}ush(\rho_i) = T_{a_{i-1}} T_{a_i}^{-1}.$$

For the τ_i curves we need to find an annular boundary to work with. We introduce the longitudinal homology curves b_i , which enclose the punctures $1, 2, \dots, i$ [“over” $1, 2, \dots, i$ and “under” $i + 1, \dots, 4$]. Thus b_0 agrees with the previous homology generator introduced, b_1 passes over puncture 1 and misses 2,3,4, and so on. The point of introducing these curves is that now τ_i has an annular neighborhood bounded by b_{i-1} and b_i . By consulting the diagrams to determine proper orientation it follows that

$$(5.5) \quad \mathcal{P}ush(\tau_i) = T_{b_i} T_{b_{i-1}}^{-1}.$$

Next we need to convert Equation 5.5 into Dehn twists only involving the homology generators given in 5.3. First we observe that we may express $[b_i] = [a_0] + [b_0] - [a_i]$, which can be verified by constructing the fundamental square for the torus with the relevant curves. An example diagram in Figure 7 is given for the $[b_1]$ case. One can straightforwardly check that $T_{a_i} T_{b_0}([a_0]) = [a_0] + [b_0] - [a_i] = [b_i]$. Fact 3.7 in [4] states $T_{f(a)} = f T_a f^{-1}$, which we can apply to our situation by setting $a = a_0$ and $f = T_{a_i} T_{b_0}$. This fact then yields

$$(5.6) \quad T_{b_i} = T_{a_i} T_{b_0} T_{a_0} T_{b_0}^{-1} T_{a_i}^{-1}.$$

FIGURE 7. Diagram for b_1 Expression

Finally, substituting formula 5.6 into equation 5.5 leads to our desired expression

$$(5.7) \quad \mathcal{P}ush(\tau_i) = T_{a_{i-1}} T_{b_0} T_{a_0}^{-1} T_{b_0}^{-1} T_{a_{i-1}}^{-1} T_{a_i} T_{b_0} T_{a_0}^{-1} T_{b_0}^{-1} T_{a_i}^{-1}.$$

REFERENCES

- [1] Joan S. Birman, *On braid groups*, Comm. Pure Appl. Math. **22** (1969), 41–72, DOI 10.1002/cpa.3160220104. MR0234447
- [2] Marc Culler, Nathan M. Dunfield, Matthias Goerner, and Jeffrey R. Weeks, *SnapPy, a computer program for studying the geometry and topology of 3-manifolds*. Available at <http://snappy.computop.org>.
- [3] David Eisenbud and Walter Neumann, *Three-dimensional link theory and invariants of plane curve singularities*, Annals of Mathematics Studies, vol. 110, Princeton University Press, Princeton, NJ, 1985. MR817982
- [4] Benson Farb and Dan Margalit, *A primer on mapping class groups*, Princeton Mathematical Series, vol. 49, Princeton University Press, Princeton, NJ, 2012. MR2850125
- [5] Matthew Gibson, *Properties of the A_∞ -structure on Primitive Forms and its Cohomology*, PhD Thesis, 2019.
- [6] Claude LeBrun, *Diffeomorphisms, symplectic forms and Kodaira fibrations*, Geom. Topol. **4** (2000), 451–456, DOI 10.2140/gt.2000.4.451. MR1796448
- [7] Curtis T. McMullen and Clifford H. Taubes, *4-manifolds with inequivalent symplectic forms and 3-manifolds with inequivalent fibrations*, Math. Res. Lett. **6** (1999), no. 5-6, 681–696, DOI 10.4310/MRL.1999.v6.n6.a8. MR1739225
- [8] Walter D. Neumann, *Splicing algebraic links*, Complex analytic singularities, Adv. Stud. Pure Math., vol. 8, North-Holland, Amsterdam, 1987, pp. 349–361. MR894301
- [9] Yongbin Ruan, *Symplectic topology on algebraic 3-folds*, J. Differential Geom. **39** (1994), no. 1, 215–227. MR1258920
- [10] Ivan Smith, *On moduli spaces of symplectic forms*, Math. Res. Lett. **7** (2000), no. 5-6, 779–788, DOI 10.4310/MRL.2000.v7.n6.a10. MR1809301
- [11] William P. Thurston, *Some simple examples of symplectic manifolds*, Proc. Amer. Math. Soc. **55** (1976), no. 2, 467–468, DOI 10.2307/2041749. MR402764
- [12] Chung-Jun Tsai, Li-Sheng Tseng, and Shing-Tung Yau, *Cohomology and Hodge theory on symplectic manifolds: III*, J. Differential Geom. **103** (2016), no. 1, 83–143. MR3488131
- [13] Li-Sheng Tseng and Shing-Tung Yau, *Cohomology and Hodge theory on symplectic manifolds: II*, J. Differential Geom. **91** (2012), no. 3, 417–443. MR2981844
- [14] Stefano Vidussi, *Homotopy $K3$'s with several symplectic structures*, Geom. Topol. **5** (2001), 267–285, DOI 10.2140/gt.2001.5.267. MR1825663
- [15] ———, *Smooth structure of some symplectic surfaces*, Michigan Math. J. **49** (2001), no. 2, 325–330, DOI 10.1307/mmj/1008719776. MR1852306

DEPARTMENT OF MATHEMATICS, UNIVERSITY OF CALIFORNIA, IRVINE, CA 92697, USA
E-mail address: gibsonmd@math.uci.edu

DEPARTMENT OF MATHEMATICS, UNIVERSITY OF CALIFORNIA, IRVINE, CA 92697, USA
E-mail address: lstseng@math.uci.edu

DEPARTMENT OF MATHEMATICS, UNIVERSITY OF CALIFORNIA, RIVERSIDE, CA 92521, USA
E-mail address: svidussi@ucr.edu